Altered cholesterol immunometabolism activates the macrophage NLRP3-inflammasome in lung fibrosis

Mariza Vaso[1], Matija Dukic[1], Peter Pennitz[2], Artür Manukyan[3], Scott Collum[4], Wanchang Lin[5], Catherine L. Winder[5], Warwick B. Dunn[5], Jonas C Schupp[6-9], Peter Braubach[10], Malgorzata Wygrecka[11], Dewei Ren[12], Erik E Suarez[12], Howard J Huang[12], Rahat Hussain[13], Bela Patel[13], Harry Karmouty-Quintana[4,12], Altuna Akalin[3], Markus Landthaler[3,14], Geraldine Nouailles[2], Matthias Ochs[1], Elena Lopez-Rodriguez[1*#] and Sonia Giambelluca[1*#]

[1]Institute of Functional Anatomy, Charité - Universitätsmedizin Berlin, corporate member of Freie Universität Berlin and Humboldt-Universität zu Berlin; German Center for Lung Research (DZL), Berlin, Germany; [2]Department of Infectious Diseases, Respiratory Medicine and Critical Care, Charité – Universitätsmedizin Berlin, corporate member of Freie Universität Berlin and Humboldt-Universität zu Berlin, Berlin, Germany; [3]Berlin Institute for Medical Systems Biology of the Max-Delbrück Center (MDC-BIMSB), Berlin, Germany; [4]Department of Biochemistry and Molecular Biology, McGovern Medical School, UTHealth Houston, TX, USA; [5]Centre for Metabolomics Research, Department of Biochemistry, Cell and Systems Biology, Institute of Systems, Molecular, and Integrative Biology, University of Liverpool, Liverpool L69 7ZB, UK; [6]Department of Respiratory Medicine and Infectious Diseases, Hannover Medical School, Hannover, Germany; [7]Biomedical Research in Endstage and Obstructive Lung Disease Hannover, German Center for Lung Research, Hannover, Germany; [8]Department of Clinical Airway Research, Fraunhofer Institute for Toxicology and Experimental Medicine (ITEM), Hannover, Germany; [9]Section of Pulmonary, Critical Care and Sleep Medicine, Yale School of Medicine, New Haven, CT, United States; [10]Institute of Pathology, Hannover Medical School, German Center for Lung Research (DZL) – BREATH, Hannover, Germany; [11]Center for Infection and Genomics of the Lung (CIGL), Justus-Liebig-Universität Giessen; German Center for Lung Research (DZL), Giessen, Germany; [12]Houston Methodist J.C. Walter Jr. Transplant Center, Houston Methodist hospital, Houston, TX, USA; [13]Divisions of Critical Care, Pulmonary and Sleep Medicine, Department of Internal Medicine, McGovern Medical School, UTHealth Houston, TX, USA; [14]Institut für Biologie, Humboldt Universität zu Berlin, Berlin, Germany

*** Both authors contributed equally to this article as lead authors and supervised the work**

 # Corresponding author:

Sonia Giambelluca, PhD and Elena Lopez-Rodriguez, PD, PhD

Institute of Functional Anatomy

Charité Universitätsmedizin-Berlin
Philippstr. 11,
10115 Berlin, Germany
Email: sonia.giambelluca@charite.de and elena.lopez-rodriguez@charite.de

Author contributions

MV, MD, SG and ELR contributed to the conception and design of the work. MV, MD, PP, AM, SC, CW, WD, PB, MW, HKQ, GN, SG, ELR contributed to the acquisition, analysis or interpretation of data for the work. MV, MD, PP, AM, SC, CW, WD, PB, MW, HKQ, GN, SG, ELR contributed to the drafting the article or revising it critically for important intellectual content; and MV, MD, PP, AM, SC, CW, WD, JCS, PB, MW, HKQ, ML, AA, GN, MO, SG, ELR gave their final approval of the version to be published.

Funding and additional information

This study was funded by the Else-Kröner-Fresenius Stiftung - project ID: 2020_EKEA.160 (to EL-R), the Deutsche Forschungsgemeinschaft (DFG, German Research Foundation) - project ID: 462596862 (to SG) and project ID: 431232613-SFB1449 (to MO and GN) and the German Center for Lung Research (DZL).

Running title: Macrophage inflammasome in in lung fibrosis

Main Text Word Count: 3614

This article has an online data supplement, which is accessible from this issue's table of content online at www.atsjournals.org

Abstract

Previous research has highlighted dysregulation in lipid metabolism during lung fibrosis. However, the impact of cholesterol immunometabolism during lung fibrosis progression remains unclear but has been related to the NLRP3-inflammasome activation in cardiovascular diseases. The main objective of this work was to investigate the link between altered cholesterol metabolism and NLRP3 inflammasome activation in fibrotic lungs. Different pulmonary fibrosis patient cohorts (from 2 centers and a publicly available dataset) and a murine model of lung fibrosis (aged SP-C$^{-/-}$) were included. Expression of cholesterol metabolism proteins and cholesterol content were determined in lungs from patients and bronchoalveolar lavage fluid (BALF) cells of aging SP-C$^{-/-}$ mice. Metabolomic and lipidomic analyses were conducted in BALF and BALF cells of SP-C$^{-/-}$ versus wild-type (WT) mice. NLRP3 inflammasome components were assessed by immunoblotting, ELISA, and immunofluorescence. Lung samples from fibrosis patients showed higher cholesterol content, altered cholesterol metabolism and higher IL-18 levels, compared to controls. Moreover, key genes related to inflammasome activation and cholesterol metabolism were differentially expressed in alveolar macrophages from IPF patients. Accordingly, BALF cells of SP-C$^{-/-}$ mice showed alteration of their cholesterol metabolism and inflammasome activation with age and fibrosis development. Lipidomic analysis pointed at cholesterol esters as potential activating agent. The molecular mechanism linking cholesterol esters to NLRP3 inflammasome and fibrosis markers was confirmed *in vitro* in a human macrophage model. In conclusion, altered cholesterol esterification activates the NLRP3 inflammasome in AM during pulmonary fibrosis in a murine model and fibrosis patients.

Word count: 246 (max 250)

Keywords: alveolar macrophages, inflammasome activation, cholesterol immunometabolism, cholesterol ester, pulmonary fibrosis, IL-18

Introduction

Idiopathic pulmonary fibrosis (IPF) is a chronic interstitial lung disease with a poor prognosis, characterized by progressive scarring of the lung, eventually leading to worsening of dyspnea and lung function, with fatal consequences for the patients. Histologically, IPF is characterised by a usual interstitial pneumonia pattern, which is defined by non-uniform and subpleural changes of lung tissue architecture associated with honeycombing and fibroblast foci formation (1, 2). Recently, progressive pulmonary fibrosis (PPF) has also been defined for pulmonary fibrosis patients (other than IPF) with worsening respiratory symptoms and evidence of disease progression (2).

In the last few years, a growing body of literature has focused on the role of lipids, and their alterations (3, 4) in the onset of pulmonary fibrosis, as extensively reviewed (5-10). Among lipids, cholesterol is the major neutral lipid in lung surfactant, where its concentration is tightly regulated, partially by alveolar macrophages (AM), via the reverse cholesterol transport (RCT) pathway (11). However, disruption in lipid homeostasis leads to lipid-laden AM, called foam cells, a common pathological feature in animal models of lung fibrosis (12, 13). From a clinical point of view, the use of cholesterol-lowering drugs seems to have controversial results in pulmonary fibrosis, with clinical trials showing a positive effect and others showing no effect (14-17). Likewise, altered cholesterol metabolism and accumulation of foam cells in lungs precede the appearance of fibrotic foci in surfactant protein C knockout (SP-C$^{-/-}$) mice, a model of sporadic age-related lung fibrosis (18). SP-C mutation is characteristic of the human familial form of interstitial pneumonia (19), and SP-C deficiency has been demonstrated in human IPF patients (20, 21).

In cardiovascular diseases, elevated cholesterol levels in circulating macrophages (22-24) eventually activate the nucleotide-binding oligomerization-(NOD)-like receptor, pyrin domain containing 3 (NLRP3) inflammasome pathway via lysosomal destabilisation (25, 26). The NLRP3 inflammasome is a multiprotein complex, formed by NLRP3, apoptosis associated speck-like protein containing a C-terminal caspase recruitment domain (ASC) and procaspase 1 (pro-Casp1). Upon activation, soluble cytoplasmic ASC oligomerizes into speck structures, which serve as a scaffold for the active caspase-1 responsible for the proteolytic cleavage of pro-interleukin 1β (pro-IL-1β) and pro-interleukin 18 into their mature forms (IL-1β and IL-18) (27, 28). The NLRP3 inflammasome was also proven to drive pulmonary fibrosis

in mice (29), most likely by an autocrine loop leading to the continual release of IL-1β and IL-18 (30).

In this study, we addressed the hypothesis that altered cholesterol metabolism may lead to activation of the NLRP3 inflammasome during lung fibrotic remodelling. The study provides a new insight on the role of cholesterol immunometabolism and alveolar macrophages as the main responsible cells for NLRP3 inflammasome activation and IL-18 production, contributing to the pathogenesis.

Materials and Methods

Detailed materials and methods are available as supplementary data.

Human patient cohorts

Patient cohort 1: Human lung tissue samples were obtained from patients (N=14) with end-stage IPF or PPF (from now on called PPF/IPF) who underwent lung transplantation at the Hannover Medical School, Hannover, Germany. Histologically normal lung tissue adjacent to tumour site was used as a healthy control (N=14). All investigations using human tissue were approved by the ethics committee of the Hannover Medical School (MHH, Hannover, Germany) and follow “The Code of Ethics of the World Medical Association” (renewed on 2015/04/22, number 2701–2015). All patients gave written informed consent for the use of their lung tissue for research. Demographics of the patients are provided in table 1.

Patient cohort 2: Formalin fixed paraffin embedded (FFPE) lung sections from IPF patients (N=12) and controls (N=6) (donors with non-lung related diseases), as described in table 2, were obtained from the UTHealth Pulmonary Centre of Excellence Biorepository. Patient consent and use of tissue were obtained after approval by the institutional review board of the UTHealth Houston with the reference number: HSC-MS-08-0354 and HSC-MS-15-1049.

An online available dataset from published patient cohorts was used and re-analysed from Adams et al 2020 (31) (Dataset GSE136831) to complete the human data analysis at the single cell level.

Study animals

SP-C$^{-/-}$ mice (background Sv129/S2) were previously described (32). Wild-type (WT) mice (background Sv129/S2) served as a control group. For metabolomic and lipidomic analyses both groups were kept under same diet conditions for at least 4 months. Approval of experimental procedures was granted by the institutional regulatory bodies ("Tierschutzbeauftragte" and "Tierschutzausschuss") at Charité Universitätsmedizin Berlin, Germany, with the permission of the local government authorities (State Office for Health and Social Affairs Berlin, Germany - LAGeSo). Bronchoalveolar lavage fluid (BALF), BALF cells and lungs from 10, 30, and 60 weeks old SP-C$^{-/-}$ and WT mice were isolated for further analysis.

Cholesterol and lipid analysis

A fluorometric assay was performed to determine the total cholesterol level, normalised by the tissue weight (mg) in human samples, the phospholipid content in BALF and protein content in BALF cells. Phospholipid content was determined by lipid extraction, followed by a colorimetric phosphorus assay. Expression of cholesterol metabolism related proteins were assessed by western blotting. Untargeted metabolomics/lipidomic analysis was performed in BALFs and BALF cells of 30 weeks old SP-C$^{-/-}$ and sex-matched WT mice.

NLRP3 activation assessment

Expression of NLRP3 inflammasome related proteins was assessed by western blotting. ASC specks were visualized by immunofluorescence, as described in supplementary methods. Concentration of IL-18 was measured in non-diluted BALFs and lung lysates by ELISA.

To investigate cholesterol-dependent NLRP3 activation, THP-1 cells were differentiated into macrophage-like cells (MLC (33)) and treated with cholesterol ester (18:1) for 48h, in presence or absence of NLRP3 inflammasome inhibitor, MCC950.

Statistical analysis

GraphPad Prism version 9.5.1 (GraphPad Software, San Diego, CA, USA) was used for data analysis. Data are expressed as median. Statistical analysis was performed using a Mann-Whitney, when comparing 2 groups, and a Kruskal-Wallis nonparametric test, followed by Dunn`s multiple comparison (>2 groups). Significant p-values are depicted as asterisk (*$p<0.05$; **$p<0.01$). For lipidomics, univariate analysis was performed.

Results

PPF/IPF patients exhibit altered lung cholesterol metabolism

Samples from patient cohort 1 (Table 1) were used to study relative amount of proteins related to cholesterol metabolism (Figure 1a-e). Statistically significant increase in LXR (Figure 1c) and decrease of CD36 (Figure 1d) were found in PPF/IPF patient samples compared to control. Moreover, there was a trend towards an increase in ApoE (Figure 1b) in PPF/IPF patient lungs. Total cholesterol content (Figure 1f) and cholesterol esters (Figure 1g) were also increased in PPF/IPF patient compared to control samples. These results indicate altered cholesterol metabolism in lungs of PPF/IPF patients.

NLRP3 inflammasome is activated in lungs and AM of different IPF and PPF patient cohorts and datasets

Samples from patient cohort 1 were also used to immunodetect protein components of the NLRP3 complex (Figure 2a). In particular, ASC and proCasp-1 (Figure 2a and Supp Figure 1e-f) showed no changes in PPF/IPF patient compared to control samples and neither NLRP3, pro-IL-1β (Figure 2a) nor IL-1β were detected in any of the samples. However, IL-18, considered the end-product of the activation of the NLRP3 inflammasome, was also significantly increased at the protein level in lung tissue lysates of PPF/IPF patients compared to control samples (Figure 2b). Together with the cholesterol ester (CE) data shown before (Figure 1g), higher IL-18 and CE was found in the PPF/IPF patient sample compared to controls (Figure 2c), suggesting a relationship between altered cholesterol metabolism and NLRP3 inflammasome activation in fibrosis. However, as ASC is constitutively expressed in many cells, we investigated the formation of the ASC-Speck, the complex formed by ASC and NLRP3 (27, 28) upon activation of this inflammasome in lung tissue.

Immunofluorescence against ASC (Figure 2d-g) showed cytosolic ASC in healthy control (Figure 2e and Supp Figure 1a) and perinuclear ASC-Speck in IPF patients (around 1µm fluorescence structures indicated by the white arrows in Figure 2f-g and Supp Figure 1a) in the patient cohort 2 (patients details in table 2) compared to secondary antibody control (Figure 2d and Supp Figure 1a). In addition, immunofluorescence of ASC and CD68 (pan-macrophage marker) (Figure 2h and 2i) showed co-localization of ASC Speck in $CD68^{+}$ cells in IPF patient samples, indicating that the activation of NLRP3 inflammasome is mostly located in macrophages (see

also Supp Figure 1a). Other lung regions, such as bronchiolar or highly remodeled regions did not show ASC speck in $CD68^-$ cells (Supp Figure 1b). Moreover, the quantification of ASC specks in $CD68^+$ cells showed increased ASC specks in IPF patient samples (Supp figure 1c) according to the increase in IL-18 release (Figure 2b).

Moreover, to confirm the findings in our sample set, open single cell sequencing data from Adams et al 2020 (31) (GSE136831), comprising lung tissue from 46 control and 32 IPF patients (Figure 2j-l), were analyzed. Cell annotations were used according to the original paper and confirmed using cell marker genes that can be found in Supp Figure 1d. Differential expression analysis of IPF versus control samples (Figure 2l) showed statistically significant over-expression of *NLRP3* and *PYCARD* (gene encoding for ASC) in AM of IPF patients, along with genes involved in cholesterol metabolism, such as *CD36*, ABCA6, and LPL. Moreover, profibrotic genes, such as genes encoding for metalloproteases (MMP-7) and collagen type 1 and 3 (COL1A1), were found to be over-expressed in AM from IPF patients. Although other cell populations showed overexpression of either cholesterol metabolism, NLRP3 inflammasome, or profibrotic genes, only AM showed overexpression of genes of the three pathways at the same time. These results indicate an interplay among cholesterol pathway, NLRP3 inflammasome, and fibrosis mediators preferentially located in AM.

Taken together, these results point at a link between cholesterol metabolism, NLRP3 inflammasome activation in alveolar macrophages in lungs of fibrotic patients.

SP-$C^{-/-}$ mice exhibit age-dependent accumulation of cholesterol esters in BALF cells

The SP-$C^{-/-}$ animal model has been previously described to spontaneously develop lung fibrosis with age by showing a combination of overdistended air spaces and fibrotic wounds, analogous to the combined emphysema and pulmonary fibrosis typical of IPF (34). Therefore, this mouse model allowed us to study cholesterol metabolism and activation of the inflammasome before and during the onset of fibrosis. Moreover, since single cell sequencing data linked and located the NLRP3 inflammasome and cholesterol metabolism genes in AMs we investigated in detail the cholesterol metabolism in BALF cells of SP-$C^{-/-}$ mice (34). Therefore, expression of proteins involved in cholesterol esterification (i.e. carboxylesterase 1 (CES1)), uptake of cholesterol (i.e. CD36), lipid droplet storage (Perilipin 1, (Plin1)), and efflux of cholesterol (liver X receptor alpha (LXRα)) were investigated in BALF cells, mainly composed

of AM (18), from 10, 30, and 60 weeks old SP-C$^{-/-}$ mice (Figure 3a). WB band densitometry (Figure 3b-d) showed statistically significant higher protein content of LXRα in the 60 weeks group (Figure 3d). Whereas CES1 and CD36 were elevated at 30 weeks of age (Figure 3b and 3c) then decreased at 60 weeks of age, correlating with the fibrotic onset in this murine model and consistent with the human data presented above. No significant changes were observed in Plin1 with aging. Furthermore, total cholesterol and cholesterol esters were quantified in BALF (Figure 3e and 3f) and BALF cells (Supp Figure 2a) of 10, 30, and 60 weeks SP-C$^{-/-}$and WT mice (Supp Figure 2b and 2c). BALF of SP-C$^{-/-}$ mice showed increasing total cholesterol (Figure 3e) and cholesterol esters (Figure 3f) with age and higher total cholesterol level compared to the WT group (Supp Figure 2c). BALF cell cholesterol decreased with age in SP-C$^{-/-}$ and WT mice (Supp Figure 2a and 2c, respectively). Moreover, we performed a metabolomic and lipidomic analysis in 30 weeks old mice BALF and BALF cells. A total of 561 and 120 metabolites in BALF cells and BALF, respectively, were present at statistically significant different levels in SP-C$^{-/-}$ compared to WT mice (Supp Figure 2e and 2f). Among these metabolites, 96% and 88% respectively, were lipids, indicating substantial variations predominantly in lipid metabolism (Figure 3g). In terms of cholesterol metabolism, data revealed a up to 3-fold increase of three cholesterol esters (CE) (CE18:1, CE19:0, CE22:6) in SP-C$^{-/-}$ mice (Figure 3h). Also, overall increases of lipid species involved in the cytidine diphosphate-diacylglycerol pathway, triglycerides, cardiolipins and ceramides were observed. Taken together, these results point at an altered lipid and cholesterol metabolism in AM of aging SP-C$^{-/-}$ mice, with an increase in CE species.

NLRP3 inflammasome is activated in AM of aging SP-C$^{-/-}$ mice

The NLRP3 inflammasome activation pathway was investigated by immunoblotting in BALF cell lysates from 10, 30, and 60 weeks old SP-C$^{-/-}$ mice (Figure 4a-e). A significant increase in NLRP3 (Figure 4b) and pro-Casp1 (Figure 4d) was accompanied by a tendency to lower intracellular soluble ASC and IL-18 (Figure 4c and 4e) with aging. Concentrations of IL-18 were found to be higher in BALF of 60 weeks old SP-C$^{-/-}$ mice (Figure 4f) and up to 1.5-fold increase compared to WT (Supp Figure 2d), indicating an elevated release with aging. Furthermore, ASC speck was visualized in BALF cells (Figure 4g) of the 60 weeks old group, demonstrating activation of NLRP3 inflammasome at the onset of fibrosis in the SP-C$^{-/-}$ mouse model (34).

AM are the main leukocyte population activating the NLRP3 inflammasome and source of IL-1β

The 60 weeks old SP-C$^{-/-}$ mice group showed increased released IL-18 and CE in BALF (Figure 5a), suggesting again a relationship between altered cholesterol metabolism and NLRP3 inflammasome in fibrotic lungs. Yet again ASC is constitutively expressed in many cells, we further wanted to pin down the cell population activating the NLRP3 inflammasome.

After harvesting the BALF cells, the viability was assessed by dye exclusion assay with trypan blue. The viability of the BALF cells resulted in 97.8 ± 0.7% for the 10 weeks old group, 98.6 ± 0.6% for the 30 weeks old group and 98.1 ± 0.7% for the 60 weeks old group. The localization of ASC among the leukocyte populations was then investigated by flow cytometry. The analysis of lung leukocytes showed that ASC was associated to the AM population (Figure 5b-d and Supp Figure 3a-b), with the CD11b^{+} macrophage population increasing with age. Percentage of AM positive for ASC was increased at the age of 60 weeks (Figure 5c), even though the total number of ASC positive AM was not increased (Figure 5d). Together with the above presented data in isolated BALF cells, these results point at activation of the NLRP3 inflammasome in aging mice, preferentially located in AM.

To explore the link between the NLRP3 inflammasome activation to the accumulation of cholesterol esters in BALF cells, we incubated differentiated human MLC (PMA-differentiated THP-1 after 24h rest (35)) with cholesteryl oleate (CE18:1) for 48h, in the presence or absence of an NLRP3-inhibitor (MCC950). As result of the inflammasome activation, IL-1β release into the medium was assessed by ELISA and shown in figure 5e. The presence of MCC950 effectively inhibited the release of IL-1β in the presence of CE, confirming the NLRP3-dependent activation of the inflammasome by cholesteryl oleate. Taken together these results point at an activation of the NLRP3 inflammasome in AM of SP-C$^{-/-}$ mice. In addition, we confirmed the CE-dependent activation of the NLRP3 inflammasome in an *in vitro* model of macrophage cells.

Discussion

In the different PPF and IPF patient cohorts studied here, evidence of altered cholesterol metabolism and NLRP3 inflammasome activation were found. In addition, the analysis of a public omics dataset from another patient cohort linked the two pathways and localized them in AM, along with upregulation of genes encoding for pro-fibrotic markers. In particular, LXR was found to be upregulated in PPF/IPF patient samples, which is normally activated by oxysterols and protects the cells from cholesterol overload by regulating RCT genes to promote cholesterol efflux (36). Moreover, CD36, which is a cholesterol transporter responsible for its uptake, was accordingly found to be down-regulated in PPF/IPF patient samples. Higher total cholesterol and cholesterol ester content in the lungs of PPF/IPF patients, compared to controls, confirmed an altered cholesterol metabolism/esterification. These data hint at the initiation of the RCT pathway as negative feedback mechanism for cholesterol overload in lungs of PPF/IPF patients. Cholesterol overload was previously correlated to NLRP3 inflammasome activation in cardiovascular diseases (25). Here, the formation of ASC speck and the accumulation of IL-18 in fibrotic lungs, compared to controls, support the activation of NLRP3 inflammasome in PPF/IPF patients. Moreover, the same set of samples used for WB of cholesterol metabolism in figure 1 was also analysed for IL-18 showing that the results from the cholesterol and NLRP3 pathways relate to each other. Another human dataset confirmed the differential expression of the inflammasome in immune cells, mainly alveolar macrophages, monocytes and dendritic cells from patients compared to controls. Moreover, the same cells showed a higher expression of genes involved in cholesterol metabolism, such as ABCA6, and in fibrogenesis, such as metalloprotease-7(37) and collagen type 1. NLRP3 inflammasome activation was also found to be related to monocytes in patients with alpha-1 antitrypsin deficiency (38). Taken together, altered cholesterol immunometabolism, with changes in cholesterol metabolism and NLRP3 inflammasome status, was a common feature in different and heterogenous patient cohorts. Of note, our data point toward AM as main actors in the activation of the NLRP3 inflammasome for the first time in lung fibrosis.

In order to investigate the changes in cholesterol metabolism and NLRP3 inflammasome in the progression of the disease, we provide supportive pre-clinical data in a murine model which spontaneously develops lung fibrosis with age (34). Moreover, the murine model

allowed us a closer examination at BALF cell level, mainly composed of AM, as preferential site for cholesterol-mediated inflammasome activation.

According to the findings in the human cohorts, BALF cells in mice clearly showed altered cholesterol metabolism and activation of the NLRP3 inflammasome with age. At the age of 30 weeks, a lipidomic analysis of the BALF cells evidenced three cholesterol ester species being 3-fold higher in the SP-C$^{-/-}$ compared to their age-matched WT controls. The cholesterol ester species elevated in the SP-C$^{-/-}$ mice, CE18:1, and CE22:6, have been related to atherosclerotic plaques, where NLRP3 inflammasome activation have also been reported (39). Along with changes in cholesterol metabolism, we found upregulation of NLRP3-related protein and ASC-speck in BALF cells, and increased levels of IL-18 in BALF of 60-weeks old mice, confirming the activation of the inflammasome. Of note, this age correspond to the formation of fibrotic foci in this model, as described before (18).

In accordance with our data, Lasithiotaki et al (2016) (40) also showed higher IL-18 in supernatants of non-stimulated macrophages of IPF patients compared to control patients. Moreover, upon canonical inflammasome stimulation with LPS+ATP, IPF BALF macrophage cultures showed increased IL-18 secretion, but not IL-1β. The IL-18 secretion increase is however inhibited in the presence of caspase-1 inhibitor, demonstrating that human alveolar macrophages can produce and release IL-18 following in vitro stimulation of the NLRP3 inflammasome activation (40). In sarcoidosis, NLRP3 inflammasome activation was also demonstrated as increase in IL-1β in unstimulated BALF cells (41). In contrast, in agreement with Jäger et al (2021) (42), under unstimulated conditions, BALF cells from healthy and IPF patients showed no differences in the release of IL-1β. However, in contrast to the reported presence of cleaved caspase 1, we were not able to detect the 20kDa, but the 50kDa pro-Casp1 form of the enzyme responsible of the transformation of the precursors into the mature forms of IL-1β and IL-18. While the IL-1β precursor is not constitutively expressed in the cells, the IL-18 precursor is found in many cells, including immune and epithelial cells. In addition, it was also described that IL-18 expression is stimulated and sustained after NLRP3 inflammasome activation, whereas IL-1β was induced but not sustained (43). IL-18 has been already linked to IPF before (44, 45), without mentioning its origin. In addition, the caspase 1-independent processing of IL-1β and IL-18 after NLRP3 inflammasome activation was already shown (46). Our clinical and preclinical data support the activation of the NLRP3

inflammasome as a potential origin of IL-18 in lung fibrosis progression. In addition, our data points at AM as the population responsible for NLRP3 activation in both humans and in mice. The potential role of cholesterol esters in the activation of the NLRP3 inflammasome was also confirmed *in vitro*. Accordingly, human cell macrophage models release IL-1β after exposure with CE. The addition of MCC950, confirmed the dependence on the NLRP3-inflammasome pathway. However, the effect *in vitro* is limited by the lack of a classical NLRP3-priming stimuli (such as LPS, DAMPs or PAMPs), but the presence of PMA, known to prime MLCs increasing the pro-IL-1β production (33), which may explain the preference in IL-1β release and not IL-18. *In vivo*, however, the co-existence of AM and inflammatory (MHCII+) macrophages, may contribute with the right niche to amplify the activation of NLRP3 at the alveoli.

The impact of cholesterol immunometabolism in the lung or during fibrosis progression remains unclear. Our data supports an association between cholesterol metabolism and immune activation of macrophages through the NLRP3 inflammasome. The molecular mechanism of immune activation by cholesterol metabolism signalling has been previously described in experimental models and cell lines (26, 47-50). In conclusion, we collected here evidence for the association of altered cholesterol metabolism and the activation of the NLRP3 inflammasome in IPF and PPF patients. In addition, preclinical data suggest that cholesterol esters may play a key role in activating the inflammasome in AM, resulting in increased release of IL-18 in the development of fibrosis. This opens up new targeted therapeutic options, not only to specific cell populations, but also to a specific immunometabolic pathway in lung fibrosis.

377 **Tables:**

378 **Table 1: Details of patient cohort 1**

Anonymized sample ID	Age (years)	Sex	Smoking status	Disease diagnosis
GLR276	78	M	N/A	Control
GLR312	64	F	N/A	Control
GLR323	59	M	N/A	Control
GLR437	69	F	Former smoker	Control
GLR738	66	F	Former smoker	Control
GLR945	57	M	Smoker	Control
GLR35	70	F	N/A	Control
GLR39	62	M	Former smoker	Control
GLR119	70	M	Smoker	Control
GLR276	78	M	N/A	Control
GLR786	54	M	Smoker	Control
GLR861	65	M	N/A	Control
GLR961	72	F	N/A	Control
GLR988	57	F	N/A	Control
GLE830	54	M	Non-smoker	PPF (EAA)
GLE997	53	M	Former smoker	PPF (sarcoidosis)
GLE1033	62	M	Former smoker	IPF
GLE1054	60	M	Former smoker	IPF
GLE1062	65	M	Former smoker	PPF (EAA)
GLE1064	55	M	Non-smoker	PPF (EAA)
GLE593	39	F	N/A	IPF
GLE733	54	M	N/A	IPF
GLE808	61	M	Non-smoker	IPF
GLE975	54	M	N/A	IPF
GLE1029	66	M	Former smoker	PPF (EAA)
GLE1036	63	M	Former smoker	PPF (SSC)
GLE1047	59	M	Former smoker	PPF (EAA)
GLE1085	49	M	Non-smoker	PPF (DIP)

379

Table 2: Details of patient cohort 2

Anonymized slide number	Age (years)	Sex	Smoking status	Disease diagnosis
1086	67	M	N/A	Control
1072	62	F	Non-smoker	Control
1063	47	F	Smoker	Control
1051	62	M	Former smoker	Control
1050	59	M	Non-smoker	Control
1041	56	M	N/A	Control
167	65	M	N/A	IPF
189	62	F	Non-smoker	IPF
104	46	F	Non-smoker	IPF
188	62	M	Non-smoker	IPF
138	65	M	Non-smoker	IPF
134	59	M	Non-smoker	IPF
171	62	M	Non-smoker	IPF
136	63	F	Non-smoker	IPF
96	46	F	Non-smoker	IPF
81	65	M	Non-smoker	IPF
110	60	F	Non-smoker	IPF
H23L060	65	M	Non-smoker	IPF

References

1. Raghu G, Remy-Jardin M, Myers JL, Richeldi L, Ryerson CJ, Lederer DJ, et al. Diagnosis of idiopathic pulmonary fibrosis. An official ATS/ERS/JRS/ALAT clinical practice guideline. Am J Respir Crit Care Med. 2018;198(5):e44–e68.
2. Raghu G, Remy-Jardin M, Richeldi L, Thomson CC, Inoue Y, Johkoh T, et al. Idiopathic pulmonary fibrosis (an update) and progressive pulmonary fibrosis in adults: an official ATS/ERS/JRS/ALAT clinical practice guideline. Am J Respir Crit Care Med. 2022;205(9):e18–e47.
3. Nambiar S, Clynick B, How BS, King A, Walters EH, Goh NS, et al. There is detectable variation in the lipidomic profile between stable and progressive patients with idiopathic pulmonary fibrosis (IPF). Respir Res. 2021;22(1):105.
4. Rindlisbacher B, Schmid C, Geiser T, Bovet C, Funke-Chambour M. Serum metabolic profiling identified a distinct metabolic signature in patients with idiopathic pulmonary fibrosis – a potential biomarker role for LysoPC. Respir Res. 2018;19(1):7.
5. Agudelo CW, Samaha G, Garcia-Arcos I. Alveolar lipids in pulmonary disease. A review. Lipids Health Dis. 2020;19(1):122.
6. Burgy O, Loriod S, Beltramo G, Bonniaud P. Extracellular lipids in the lung and their role in pulmonary fibrosis. Cells. 2022;11(7):1209.
7. Chen R, Dai J. Lipid metabolism in idiopathic pulmonary fibrosis: From pathogenesis to therapy. J Mol Med. 2023;101(8):905–15.
8. Mamazhakypov A, Schermuly RT, Schaefer L, Wygrecka M. Lipids - two sides of the same coin in lung fibrosis. Cell Signal. 2019;60:65–80.
9. Suryadevara V, Ramchandran R, Kamp DW, Natarajan V. Lipid mediators regulate pulmonary fibrosis: potential mechanisms and signaling pathways. Int J Mol Sci. 2020;21(12):4257.
10. Tian Y, Duan C, Feng J, Liao J, Yang Y, Sun W. Roles of lipid metabolism and its regulatory mechanism in idiopathic pulmonary fibrosis: A review. Int J Biochem Cell Biol. 2023;155:106361.
11. Wygrecka M, Alexopoulos I, Potaczek DP, Schaefer L. Diverse functions of apolipoprotein A-I in lung fibrosis. Am J Physiol Cell Physiol. 2023;324(2):C438–C46.
12. Romero F, Shah D, Duong M, Penn RB, Fessler MB, Madenspacher J, et al. A pneumocyte–macrophage paracrine lipid axis drives the lung toward fibrosis. Am J Respir Cell Mol Biol. 2015;53(1):74–86.
13. Venosa A, Smith LC, Murray A, Banota T, Gow AJ, Laskin JD, et al. Regulation of macrophage foam cell formation during nitrogen mustard (NM)-induced pulmonary fibrosis by lung lipids. Toxicol Sci. 2019;172(2):344–58.
14. Andreikos D, Karampitsakos T, Tzouvelekis A, Stratakos G. Statins' still controversial role in pulmonary fibrosis: What does the evidence show? Pulm Pharmacol Ther. 2022;77:102168.
15. Kim JW, Rhee CK, Kim TJ, Kim YH, Lee SH, Yoon HK, et al. Effect of pravastatin on bleomycin-induced acute lung injury and pulmonary fibrosis. Clin Exp Pharmacol Physiol. 2010;37(11):1055–63.
16. Kreuter M, Bonella F, Maher TM, Costabel U, Spagnolo P, Weycker D, et al. Effect of statins on disease-related outcomes in patients with idiopathic pulmonary fibrosis. Thorax. 2017;72(2):148–53.
17. Lambert EM, Wuyts WA, Yserbyt J, De Sadeleer LJ. Statins: cause of fibrosis or the opposite? Effect of cardiovascular drugs in idiopathic pulmonary fibrosis. Respir Med. 2021;176:106259.
18. Ruwisch J, Sehlmeyer K, Roldan N, Garcia-Alvarez B, Perez-Gil J, Weaver TE, et al. Air space distension precedes spontaneous fibrotic remodeling and impaired cholesterol metabolism in the absence of surfactant protein C. Am J Respir Cell Mol Biol. 2020;62(4):466–78.
19. Kropski JA, Blackwell TS, Loyd JE. The genetic basis of idiopathic pulmonary fibrosis. Eur Respir J. 2015;45(6):1717–27.
20. Blumhagen RZ, Kurche JS, Cool CD, Walts AD, Heinz D, Fingerlin TE, et al. Spatially distinct molecular patterns of gene expression in idiopathic pulmonary fibrosis. Respir Res. 2023;24(1):287.
21. Markart P, Ruppert C, Wygrecka M, Schmidt R, Korfei M, Harbach H, et al. Surfactant protein C mutations in sporadic forms of idiopathic interstitial pneumonias. Eur Respir J. 2007;29(1):134 – 7.
22. Grebe A, Latz E. Cholesterol crystals and inflammation. Curr Rheumatol Rep. 2013;15(3):313.

23. Moore KJ, Sheedy FJ, Fisher EA. Macrophages in atherosclerosis: a dynamic balance. Nat Rev Immunol. 2013;13(10):709–21.
24. Varsano N, Beghi F, Elad N, Pereiro E, Dadosh T, Pinkas I, et al. Two polymorphic cholesterol monohydrate crystal structures form in macrophage culture models of atherosclerosis. Proc Natl Acad Sci. 2018;115(30):7662–9.
25. Duewell P, Kono H, Rayner KJ, Sirois CM, Vladimer G, Bauernfeind FG, et al. NLRP3 inflammasomes are required for atherogenesis and activated by cholesterol crystals. Nature. 2010;464(7293):1357—61.
26. Rajamäki K, Lappalainen J, Öörni K, Välimäki E, Matikainen S, Kovanen PT, et al. Cholesterol crystals activate the NLRP3 inflammasome in human macrophages: a novel link between cholesterol metabolism and inflammation. PLoS One. 2010;5(7):e11765.
27. Akbal A, Dernst A, Lovotti M, Mangan MSJ, McManus RM, Latz E. How location and cellular signaling combine to activate the NLRP3 inflammasome. Cell Mol Immunol. 2022;19(11):1201–14.
28. McKee CM, Coll RC. NLRP3 inflammasome priming: A riddle wrapped in a mystery inside an enigma. J Leukoc Biol. 2020;108(3):937–52.
29. Gasse P, Mary C, Guenon I, Noulin N, Charron S, Schnyder-Candrian S, et al. IL-1R1/MyD88 signaling and the inflammasome are essential in pulmonary inflammation and fibrosis in mice. The Journal of Clinical Investigation. 2007;117(12):3786–99.
30. Artlett CM. The mechanism and regulation of the NLRP3 inflammasome during fibrosis. Biomolecules. 2022;12(5):634.
31. Adams TS, Schupp JC, Poli S, Ayaub EA, Neumark N, Ahangari F, et al. Single-cell RNA-seq reveals ectopic and aberrant lung-resident cell populations in idiopathic pulmonary fibrosis. Science Advances. 2020;6(28):eaba1983.
32. Glasser SW, Burhans MS, Korfhagen TR, Na CLL, Sly PD, Ross GF, et al. Altered stability of pulmonary surfactant in SP-C-deficient mice. Proceedings of the National Academy of Sciences. 2001;98(11):6366–71.
33. Giambelluca S, Ochs M, Lopez-Rodriguez E. Resting time after phorbol 12-myristate 13-acetate in THP-1 derived macrophages provides a non-biased model for the study of NLRP3 inflammasome. Front Immunol. 2022;13:958098.
34. Ruwisch J, Sehlmeyer K, Roldan N, Garcia-Alvarez B, Perez-Gil J, Weaver TE, et al. Air space distension precedes spontaneous fibrotic remodeling and impaired cholesterol metabolism in the absence of surfactant protein C. Am J Respir Cell Mol Biol. 2020;62(4):466–78.
35. Giambelluca S, Ochs M, Lopez-Rodriguez E. Resting time after phorbol 12-myristate 13-acetate in THP-1 derived macrophages provides a non-biased model for the study of NLRP3 inflammasome. Front Immunol. 2022;13:958098.
36. Fu X, Menke JG, Chen Y, Zhou G, MacNaul KL, Wright SD, et al. 27-Hydroxycholesterol is an endogenous ligand for liver X receptor in cholesterol-loaded cells. J Biol Chem. 2001;276(42):38378–87.
37. Mckeown S, Richter AG, O'Kane C, Mcauley DF, Thickett DR. MMP expression and abnormal lung permeability are important determinants of outcome in IPF. Eur Respir J. 2009;33(1):77–84.
38. Gogoi D, Yu H, Casey M, Baird R, Yusuf A, Forde L, et al. Monocyte NLRP3 inflammasome and interleukin-1β activation modulated by alpha-1 antitrypsin therapy in deficient individuals. Thorax. 2024:thorax–2023–221071.
39. Stegemann C, Drozdov I, Shalhoub J, Humphries J, Ladroue C, Didangelos A, et al. Comparative lipidomics profiling of human atherosclerotic plaques. Circ Cardiovasc Genet. 2011;4(3):232–42.
40. Lasithiotaki I, Giannarakis I, Tsitoura E, Samara KD, Margaritopoulos GA, Choulaki C, et al. NLRP3 inflammasome expression in idiopathic pulmonary fibrosis and rheumatoid lung. Eur Respir J. 2016;47(3):910–8.
41. Huppertz C, Jäger B, Wieczorek G, Engelhard P, Oliver SJ, Bauernfeind F-G, et al. The NLRP3 inflammasome pathway is activated in sarcoidosis and involved in granuloma formation. Eur Respir J. 2020;55(3):1900119.

42. Jäger B, Seeliger B, Terwolbeck O, Warnecke G, Welte T, Müller M, et al. The NLRP3-inflammasome-caspase-1 pathway is upregulated in idiopathic pulmonary fibrosis and acute exacerbations and is inducible by apoptotic A549 cells. Front Immunol. 2021;12.
43. Zhu Q, Kanneganti T-D. Cutting Edge: Distinct Regulatory Mechanisms Control Proinflammatory Cytokines IL-18 and IL-1β. The Journal of Immunology. 2017;198(11):4210–5.
44. Kitasato Y, Hoshino T, Okamoto M, Kato S, Koda Y, Nagata N, et al. Enhanced expression of interleukin-18 and its receptor in idiopathic pulmonary fibrosis. Am J Respir Cell Mol Biol. 2004;31(6):619–25.
45. Nakanishi Y, Horimasu Y, Yamaguchi K, Sakamoto S, Masuda T, Nakashima T, et al. IL-18 binding protein can be a prognostic biomarker for idiopathic pulmonary fibrosis. PLoS One. 2021;16(6):e0252594.
46. Mehta VB, Hart J, Wewers MD. ATP-stimulated release of interleukin (IL)-1β and IL-18 requires priming by lipopolysaccharide and is independent of caspase-1 cleavage. J Biol Chem. 2001;276(6):3820–6.
47. Dang EV, McDonald JG, Russell DW, Cyster JG. Oxysterol restraint of cholesterol synthesis prevents AIM2 inflammasome activation. Cell. 2017;171(5):1057–71.e11.
48. de la Roche M, Hamilton C, Mortensen R, Jeyaprakash AA, Ghosh S, Anand PK. Trafficking of cholesterol to the ER is required for NLRP3 inflammasome activation. J Cell Biol. 2018;217(10):3560–76.
49. Guo C, Chi Z, Jiang D, Xu T, Yu W, Wang Z, et al. Cholesterol homeostatic regulator SCAP-SREBP2 integrates NLRP3 inflammasome activation and cholesterol biosynthetic signaling in macrophages. Immunity. 2018;49(5):842–56.e7.
50. Hayakawa S, Tamura A, Nikiforov N, Koike H, Kudo F, Cheng Y, et al. Activated cholesterol metabolism is integral for innate macrophage responses by amplifying Myd88 signaling. JCI Insight. 2022;7(22).

Table legends

Table 1: **Details of patient cohort 1.** ID: identification; M: male; F: female; IPF: idiopathic pulmonary fibrosis; PPF: progressive pulmonary fibrosis; EAA: extrinsic allergic alveolitis; SSC: systemic sclerosis; DIP: desquamative interstitial pneumonia; N/A: not available.

Table 2: **Details of patient cohort 2.** M: male; F: female; IPF: idiopathic pulmonary fibrosis; N/A: not available.

Figure legends

Figure 1: **Altered cholesterol metabolism in PPF/ IPF patients.** a) Representative WB of ApoE, LXR, CD36 and LDLR with their corresponding loading control (β-actin) in control (N=6) and PPF/IPF (N=6) patient lung tissue samples. A technical positive control (OxLDL+), cell lysate of PMA-differentiated THP-1 cells treated with OxLDL, as described in the supp methods section, was added to confirm specificity of the band analysed. Band densitometry corrected by β-actin of b) ApoE c) LXR, d) CD36, e) LDLR. f) Total cholesterol and g) cholesterol esters in lung tissue of control (N=6) and PPF/IPF (N=6) patients. Data presented as median, non-parametric Mann Whitney test, *p<0.05, **p< 0.01 statistically significant.

Figure 2: **Activation of NLRP3 inflammasome in different PPF and IPF patient cohorts**. a) secreted IL-18 and CE (µM/mg tissue) in lung tissue samples of control and PPF/IPF patients. Group average and standard deviation (error bars) of N=6 per group for CE and N=12 for IL-18. b) Representative WB of NLRP3, ASC, pro-Casp1 and pro-IL-1β with their corresponding loading control (β-actin) in lung tissue from control (N=6) and PPF/IPF (N=6) patients. A technical positive control (PMA-differentiated THP-1 cells treated with LPS and NIG, as described in the supp methods section, Ctrl+) was added to confirm specificity of the band analyzed. c) IL-18 in lung tissue from control (N=12) and PPF/IPF (N=12) and samples. Data are normalized by total protein content and presented as median, non-parametric Mann Whitney test, *p<0.05, **p< 0.01 statistically significant. d-g) Representative immunofluorescence staining of cytosolic ASC (white) and ASC-Speck (white arrow, activated complex of ASC and NLRP3) in d) secondary antibody control; e) healthy control and; f) IPF patient (scale bar= 20µm), with a g) high magnification picture of the ASC speck. h-i) Co-localization of ASC in

544 macrophages. Immunofluorescence staining of CD68 (red), ASC (white) in h) a healthy control
545 and i) and IPF sample. j-l) single cell sequencing data from Adams et al 2020 (Dataset
546 GSE136831) with j) patient cohort details, k) UMAP plot with cell annotations and l) dot plot
547 indicating statistically significant differentially expressed genes of the NLRP3-inflammasome
548 and cholesterol metabolism pathway. The color code indicates the average logarithmic 2-fold
549 change (log2FoldChange) and the dot size, the the absolute log2FoldChange in the comparison
550 of control vs IPF samples. AT= alveolar type; cDC= classical dendritic cell; NK= natural killer;
551 VE= vascular endothelial; cMonocyte= classical monocyte; B=B lymphocytes; T= T
552 lymphocytes.
553

554 Figure 3: **SP-C$^{-/-}$ mice exhibit age-dependent alteration in cholesterol metabolism and**
555 **accumulation of cholesterol in BALF.** a) Representative WB of CES1, CD36, and LXR-alpha
556 (LXRα) with their corresponding loading control (β-actin) in BALF cells of SP-C$^{-/-}$ mice at 10, 30
557 and 60 weeks of age. WB band densitometry corrected by β-actin of b) CES1, c) CD36, and d)
558 LXRα in SP-C$^{-/-}$ mice at 10, 30 and 60 weeks of age. e) Cholesterol and f) cholesterol esters
559 normalized by phospholipid (PL) in BALF from SP-C$^{-/-}$ mice at 10, 30 and 60 weeks of age. Data
560 presented as median; Kruskal-Wallis followed by Dunn`s multiple comparisons test, *p<0.05,
561 **p< 0.01 statistically significant. g) Representative lipidomic analysis showing lipid classes at
562 increased level in BALF cells from 30 weeks old SP-C$^{-/-}$ mice compared to WT controls. h) Main
563 cholesterol metabolism related species increased in BALF cells in SP-C$^{-/-}$ 30 weeks old mice
564 compared to WT controls. CE = cholesterol ester.
565

566 Figure 4: **Expression of NLRP3 inflammasome components, IL-18 extracellular release and**
567 **ASC oligomerization confirm inflammasome activation in aging SP-C$^{-/-}$ mice.** a)
568 Representative immunoblots of NLRP3 inflammasome related protein levels in BALF cells from
569 10, 30, and 60 weeks old SP-C$^{-/-}$ mice (N=4 mice/group) with their corresponding loading
570 control (β-actin). WB densitometric analysis of b) NLRP3, c) ASC, d) pro-Casp1 and e) IL-18 level
571 to β-actin (as loading control). f) IL-18 extracellular release assessed by ELISA in BALF samples
572 of 10, 30, and 60 weeks old SP-C$^{-/-}$ mice (N=6 mice/group). Kruskal-Wallis followed by Dunn`s
573 multiple comparisons test, *p<0.05, **p< 0.01 statistically significant. g) Immunofluorescence
574 staining of cytosolic ASC and ASC-Speck (white arrow, activated complex of ASC and NLRP3) in

60 weeks old SP-C$^{-/-}$ mice (upper panels) and secondary antibody control (lower panels), scale bar=20µm.

Figure 5: **AM in aging mice are the leukocyte population activating NLRP3-inflammasome and exposure of macrophage cell models to CE showed IL-1β NLRP3-dependent release.** a) secreted IL-18 and CE (CE/PL) in BALF from aging SP-C$^{-/-}$ mice. Group average and standard deviation of N=5 per age group. b-d) Flow cytometry analysis of immune cells upregulating inflammasome components. b) Number of lung leukocytes, mainly AM, F40/80^{lo} CD11b^{+} interstitial macrophages (iM), containing Ly6C^{high} and MHCII^{+} iMs. Percentage c) and number d) of ASC^{+} AM in different age groups. e) IL-1β concentration in medium of MLC exposed to CE in the presence or absence of MCC950 for 48h (ND=not detected).

Data availability

Data will be made available by the authors, upon reasonable request.

The code used for data analysis is available through github.com at https://github.com/Lopez-Giambelluca/LungChol.

Supporting information

This article has an online data supplement, which is accessible from this issue's table of content online at www.atsjournals.org

Acknowledgements

The authors thank Kerstin Riskowsky, Frauke Grams, John Horn and Katja Dörfel (Institute of Functional Anatomy, Charité – Universitätsmedizin Berlin, Germany), and Petra Schrade (Core Facility Electron Microscopy, Charité – Universitätsmedizin Berlin, Germany), for excellent technical assistance. We thank the Core Facility for Electron Microscopy of the Charité for support in acquisition of the data.

Conflict of interest

603 MV, MD, PP, AM, SC, WBD, CLW, WL, ML, AA, MO, SG and ELR declare no conflict of interest.
604 JCS discloses support from MSD, Boehringer, Ann Theodore Foundation, and Kinevant. HKQ
605 discloses support from NHLBI. Independent of this work, GN has received project funding from
606 Biotest AG.

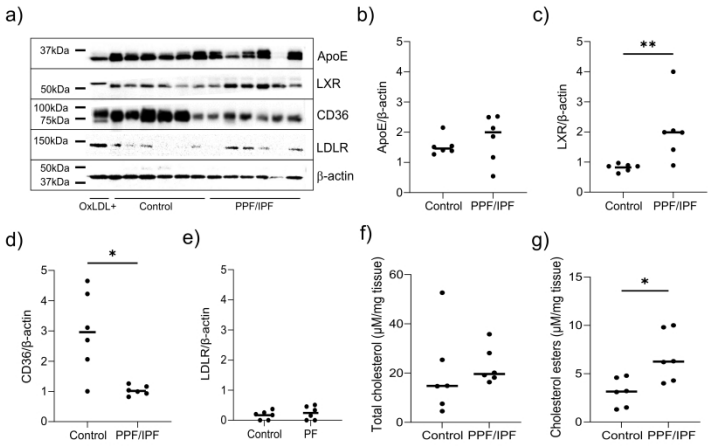

Figure 1: Altered cholesterol metabolism in PPF/ IPF patients. a) Representative WB of ApoE, LXR, CD36 and LDLR with their corresponding loading control (β-actin) in control (N=6) and PPF/IPF (N=6) patient lung tissue samples. A technical positive control (OxLDL+), cell lysate of PMA-differentiated THP-1 cells treated with OxLDL, as described in the supp methods section, was added to confirm specificity of the band analysed. Band densitometry corrected by β-actin of b) ApoE c) LXR, d) CD36, e) LDLR. f) Total cholesterol and g) cholesterol esters in lung tissue of control (N=6) and PPF/IPF (N=6) patients. Data presented as median, non-parametric Mann Whitney test, *p<0.05, **p< 0.01 statistically significant.

533x755mm (236 x 236 DPI)

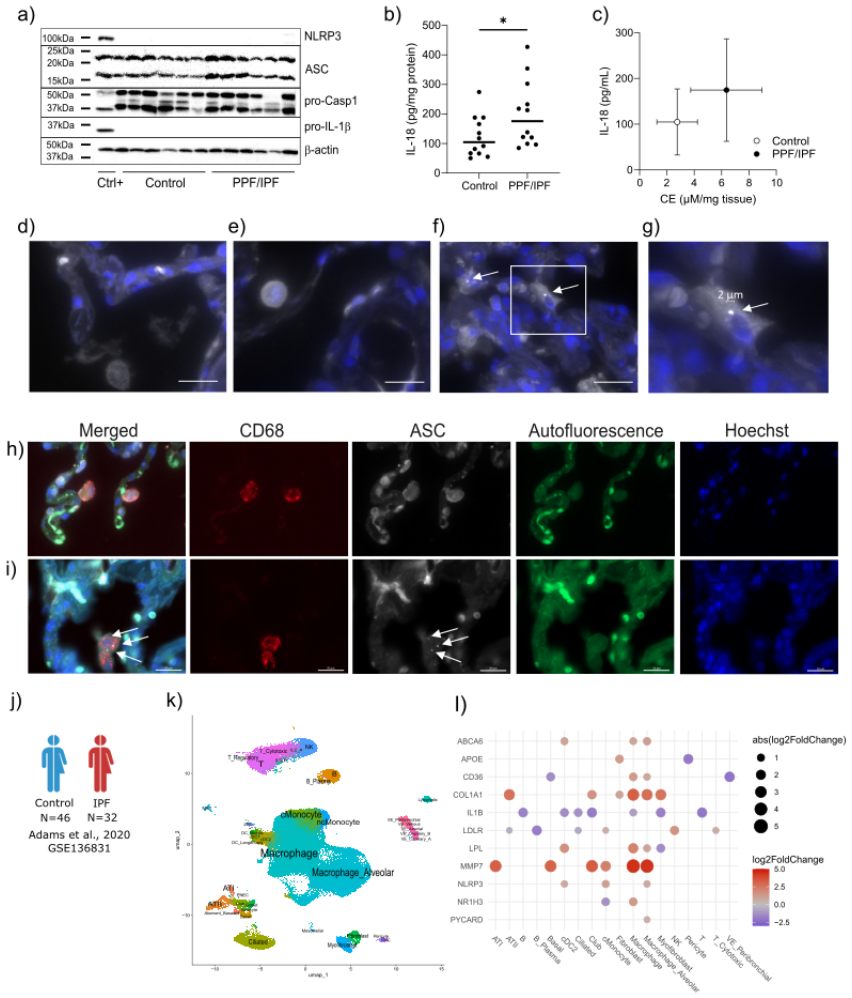

Figure 2: Activation of NLRP3 inflammasome in different PPF and IPF patient cohorts. a) secreted IL-18 and CE (µM/mg tissue) in lung tissue samples of control and PPF/IPF patients. Group average and standard deviation (error bars) of N=6 per group for CE and N=12 for IL-18. b) Representative WB of NLRP3, ASC, pro-Casp1 and pro-IL-1β with their corresponding loading control (β-actin) in lung tissue from control (N=6) and PPF/IPF (N=6) patients. A technical positive control (PMA-differentiated THP-1 cells treated with LPS and NIG, as described in the supp methods section, Ctrl+) was added to confirm specificity of the band analyzed. c) IL-18 in lung tissue from control (N=12) and PPF/IPF (N=12) and samples. Data are normalized by total protein content and presented as median, non-parametric Mann Whitney test, *p<0.05, **p< 0.01 statistically significant. d-g) Representative immunofluorescence staining of cytosolic ASC (white) and ASC-Speck (white arrow, activated complex of ASC and NLRP3) in d) secondary antibody control; e) healthy control and; f) IPF patient (scale bar= 20µm), with a g) high magnification picture of the ASC speck. h-i) Co-localization of ASC in macrophages. Immunofluorescence staining of CD68 (red), ASC (white) in h) a healthy control and i) and IPF sample. j-l) single cell sequencing data from Adams et al 2020 (Dataset GSE136831) with j) patient cohort details, k) UMAP plot with cell annotations and l) dot plot indicating

statistically significant differentially expressed genes of the NLRP3-inflammasome and cholesterol metabolism pathway. The color code indicates the average logarithmic 2-fold change (log2FoldChange) and the dot size, the absolute log2FoldChange in the comparison of control vs IPF samples. AT= alveolar type; cDC= classical dendritic cell; NK= natural killer; VE= vascular endothelial; cMonocyte= classical monocyte; B=B lymphocytes; T= T lymphocytes.

530x750mm (38 x 38 DPI)

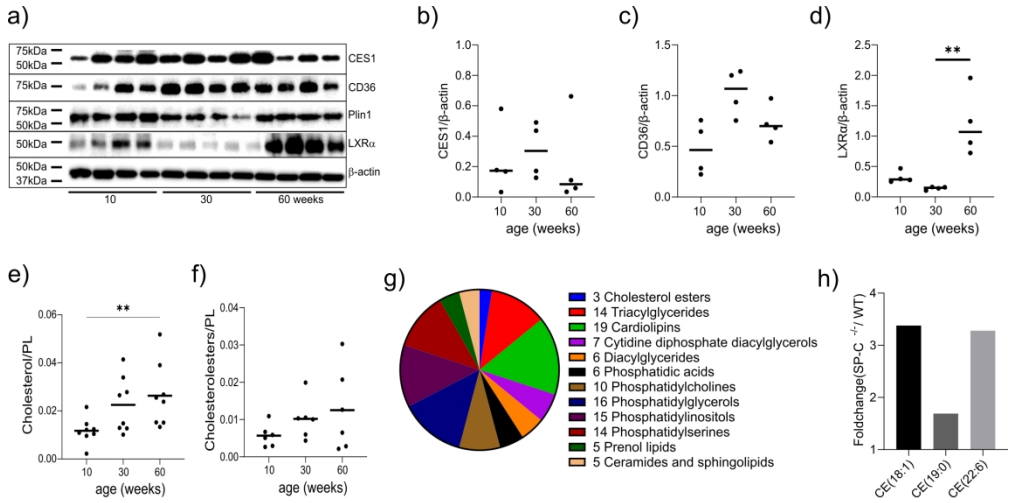

Figure 3: SP-C–/– mice exhibit age-dependent alteration in cholesterol metabolism and accumulation of cholesterol in BALF. a) Representative WB of ACAT1, CES1, CD36, and LXR-alpha (LXRα) with their corresponding loading control (β-actin) in BALF cells of SP-C–/– mice at 10, 30 and 60 weeks of age. WB band densitometry corrected by β-actin of b) ACAT1, c) CES1, d) CD36, and e) LXRα in SP-C–/– mice at 10, 30 and 60 weeks of age. f) Cholesterol and g) cholesterol esters normalized by phospholipid (PL) in BALF from SP-C–/– mice at 10, 30 and 60 weeks of age. Data presented as median; Kruskal-Wallis followed by Dunn`s multiple comparisons test, *p<0.05, **p< 0.01 statistically significant. h) Representative lipidomic analysis showing lipid classes at increased level in BALF cells from 30 weeks old SP-C–/– mice compared to WT controls. i) Main cholesterol metabolism related species increased in BALF cells in SP-C–/– 30 weeks old mice compared to WT controls. CE = cholesterol ester.

515x254mm (118 x 118 DPI)

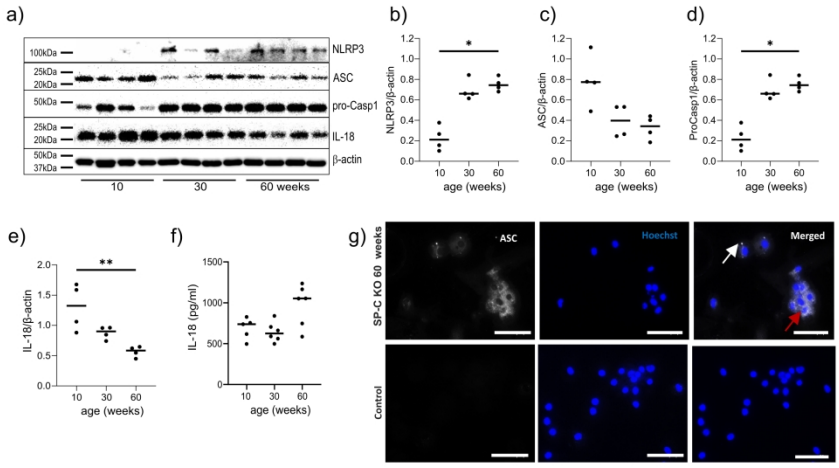

Figure 4: Expression of NLRP3 inflammasome components, IL-18 extracellular release and ASC oligomerization confirm inflammasome activation in aging SP-C–/– mice. a) Representative immunoblots of NLRP3 inflammasome related protein levels in BALF cells from 10, 30, and 60 weeks old SP-C–/– mice (N=4 mice/group) with their corresponding loading control (β-actin). WB densitometric analysis of b) NLRP3, c) ASC, d) pro-Casp1 and e) IL-18 level to β-actin (as loading control). f) IL-18 extracellular release assessed by ELISA in BALF samples of 10, 30, and 60 weeks old SP-C–/– mice (N=6 mice/group). Kruskal-Wallis followed by Dunn`s multiple comparisons test, *p<0.05, **p< 0.01 statistically significant. g) Immunofluorescence staining of cytosolic ASC and ASC-Speck (white arrow, activated complex of ASC and NLRP3) in 60 weeks old SP-C–/– mice (upper panels) and secondary antibody control (lower panels), scale bar=20μm.

533x755mm (118 x 118 DPI)

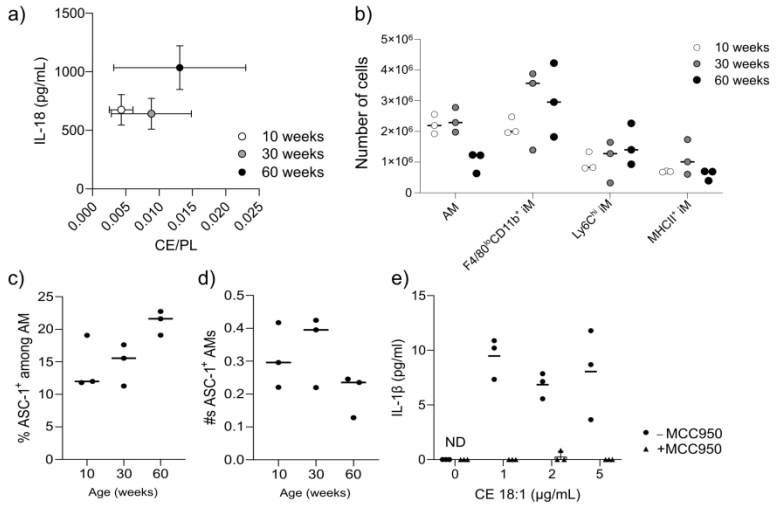

Figure 5: AM in aging mice are the leukocyte population activating NLRP3-inflammasome and exposure of macrophage cell models to CE showed IL-1β NLRP3-dependent release. a) secreted IL-18 and CE (CE/PL) in BALF from aging SP-C–/– mice. Group average and standard deviation of N=5 per age group. b-d) Flow cytometry analysis of immune cells upregulating inflammasome components. b) Number of lung leukocytes, mainly AM, F40/80lo CD11b+ interstitial macrophages (iM), containing Ly6Chigh and MHCII+ iMs. Percentage c) and number d) of ASC+ AM in the different age groups. e) IL-1β concentration in medium of MLC exposed to CE in the presence or absence of MCC950 for 48h (ND=not detected).

533x755mm (118 x 118 DPI)